Detection of SARS-CoV-2 in COVID-19 Patient Nasal Swab Samples Using Signal Processing

Mahmoud Al Ahmad, *Senior Member, IEEE*, Lillian J. A. Olule, *Member, IEEE*, Mohammed Meetani, Farrukh Amin Sheikh, Rahima Al Blooshi, Neena G. Panicker, Farah Mustafa, and Tahir A. Rizvi

***Abstract*—This work presents an opto-electrical method that measures the viral nucleocapsid protein and anti-N antibody interactions to differentiate between SARS-CoV-2 negative and positive nasal swab samples. Upon light exposure of the patient nasal swab sample mixed with the anti-N antibody, charge transfer (CT) transitions within the altered protein folds are initiated between the charged amino acids side chain moieties and the peptide backbone that play the role of donor and acceptor groups. A Figure of Merit (FOM) was introduced to correlate the relative variations of the samples with and without antibody at two different voltages. Empirically, SARS-CoV-2 in patient nasal swab samples was detected within two minutes, if an extracted FOM threshold of >1 was achieved; otherwise, the sample was considered negative.**

***Index Terms*—COVID-19, light intensity, nucleocapsid protein, optical detection, SARS-CoV-2.**

I. Introduction

THE CORONAVIRUS disease 2019 (COVID-19) has ravaged the global population since the end of 2019 [1]. As of December 23, 2021, over 275 million cases and >5.3 million deaths have been reported worldwide [2]. This pandemic has caused massive social and economic disruptions in nearly every country and therefore global research and development efforts are being geared towards development of vaccines and therapeutics for the prevention and treatment of COVID-19, in order to normalize the situation. The novel severe acute respiratory syndrome coronavirus 2 (SARS-CoV-2) that causes COVID-19 enters the susceptible cells primarily via endocytosis using its spike (S) protein [3]–[5]. The viral S protein is a homotrimer that protrudes from the virion surface [6] and is responsible for entry into susceptible cells by binding to the human angiotensin converting enzyme 2 (ACE2) protein [3]–[5]. Once internalized, the virus starts to replicate within the cell [7]. The nucleocapsid (N) protein of SARS-CoV-2, is the largest structural protein of the virus which coats its large genomic RNA and is responsible for creating its helical structure [8]. Compared to the viral S protein, the N protein is much more conserved (∼90%), is expressed at high levels during infection, and is highly immunogenic [8].

Currently, there are two main strategies for the detection of COVID-19. The first is a real time reverse transcriptase (RT) quantitative polymerase chain reaction (RT-qPCR)-based strategy that detects the viral nucleic acid in patient samples (presence of the viral RNA). The second strategy, is an immunological assay that detects viral protein antigens or serum antibodies produced as a result of the body's immune response to the viral infection [9]–[11]. The two strategies complement each other, with the PCR strategy detecting the virus during its active phase, while the immunological assay identifies individuals who have developed antibodies to fight the disease.

RT-qPCR is considered the gold standard for performing clinical diagnostics within which the RNA sequences are amplified [12]. Nevertheless, there is an urgent demand for platforms that are rapid, accurate, simple, and portable. Several researchers have tried to come up with less time-consuming PCR-based alternative solutions. A reverse transcriptase loop-mediated isothermal amplification (RT-LAMP) nucleic acid-based detection of SARS-CoV-2 with an additively manufactured cartridge has been proposed [13]. RT LAMP is still a time consuming assay that does not require an RNA extraction kit. Recently, a fast one-pot nano PCR with RT-PCR technology for COVID-19 diagnostics has been developed [14]. The viral detection time has been reduced to 15 minutes. The system incorporates plasmonic thermo cycling with fluorescent signal detection in a single device. This PCR-based method is a relatively expensive and

Manuscript received May 16, 2021; revised October 18, 2021 and November 20, 2021; accepted December 2, 2021. Date of publication December 9, 2021; date of current version April 18, 2022. This work was supported by the Zayed Center for Health Sciences (ZCHS), UAE University under Grant 31R129. The guest editor coordinating the review of this manuscript and approving it for publication was Prof. Bjoern Schuller. *(Corresponding author: Mahmoud Al Ahmad).*

Mahmoud Al Ahmad is with the Department of Electrical Engineering, UAE University, Al Ain 15551, UAE, and also with the Zayed Center for Health Sciences (ZCHS), UAE University, Al Ain 15551, UAE (e-mail: m.alahmad@uaeu.ac.ae).

Lillian J. A. Olule is with the Department of Electrical Engineering, UAE University, Al Ain 15551, UAE (e-mail: lolule@uaeu.ac.ae).

Mohammed Meetani is with the Department of Chemistry, COS UAE University, Al Ain 15551, UAE (e-mail: mmeetani@uaeu.ac.ae).

Farrukh Amin Sheikh and Rahima Al Blooshi are with the Department of Microbiology, Al Ain Hospital, Al Ain 109090, UAE (e-mail: fsheikh@seha.ae; rbalooshi@seha.ae).

Neena G. Panicker is with the Department of Biochemistry & Molecular Biology, CMHS UAE University, Al Ain 17666, UAE (e-mail: 201990158@uaeu.ac.ae).

Farah Mustafa is with the Department of Biochemistry and Molecular Biology, CMHS UAE University, Al Ain 17666, UAE, and also with the Zayed Center for Health Sciences (ZCHS), UAE University, Al Ain 15551, UAE (e-mail: fmustafa@uaeu.ac.ae).

Tahir A. Rizvi is with the Department of Microbiology and Immunology, CMHS UAE University, Al Ain 17666, UAE, and also with the Zayed Center for Health Sciences (ZCHS), UAE University, Al Ain 15551, UAE (e-mail: tarizvi@uaeu.ac.ae).

This work involved human subjects or animals in its research. Approval of all ethical and experimental procedures and protocols was granted by Abu Dhabi Department of Health Covid-19 IRB committee under Application number: DOH/CVDC/2020/872. and performed in line with the Al Ain Hospital.

Digital Object Identifier 10.1109/JSTSP.2021.3134073

© IEEE 2021. This article is free to access and download, along with rights for full text and data mining, re-use and analysis.

time-consuming technique that needs an expert technician. In addition to PCR, the emerging gene editing-based CRISPR (clustered regularly interspaced short palindromic repeats)/Cas technologies are promising to provide faster, more sensitive, and cheaper alternatives to SARS-CoV-2 biomolecular diagnostics. The current CRISPR/Cas tests approved for emergency use still need an amplification step, but improvements are being introduced that should reduce the number of steps to achieve detection [15]–[18]. These tests are portable and use fluorescence-based detection that are coupled to smartphones to produce rapid results within 15-60 minutes. On the other hand, several researchers have tried to explore the use of biosensor devices [19], [20]. Biosensors interact with biomolecules and transduce their readings into measurable outputs, such as optical, electrical and enzymatic. A COVID-19 field-effect transistor-based (FET) sensor incorporating a graphene sheet at the sensing area has been developed [21]. The FET-based sensors require functionalization of high concentration of antibodies to have a highly responsive detection of the SARS-CoV-2 virus in clinical samples. The measurement setup is not portable and requires a calibration procedure and highly skilled personnel to run it. Another approach has been to use the dual-functional plasmonic biosensor to provide an alternative and promising solution in improving the accuracy for clinical COVID-19 diagnosis [22]. Nevertheless, the proposed technique demands surface functionalization and viral sequence detection which requires sophisticated and complex sample preparation and handling. Furthermore, the utilization of membrane-engineered mammalian cells bearing the human chimeric spike S1 antibody and the possibility for the attachment of the protein to the membrane-bound antibodies has been proposed [23]. No actual clinical validation of the assay using patient samples has been provided. The use of electro-insertion of tens of thousands of the SARS-CoV-2 spike S1 antibody into the cell membrane makes this method not a practical solution and requires sample processing and preparation. Biosensors can provide label-free, real-time detection and curtailment of non-specific binding. However, they also face the challenge of efficient immobilization of biomolecules on the sensing surface [24].

Recent reports have found distinctive UV-visible light spectra in the range of 250–800 nm for proteins rich in charged amino acids that are in monomeric form and devoid of aromatic amino acids [25]–[29]. Prasad *et al.* have shown that the protein charge transfer spectra (ProCharTS) band comprises of facile photo induced peptide backbone to side chain charge transfer and side chain to side chain charge transfer transitions in charged amino acids such as lysine (Lys) and glutamate (Glu) [28]. In fact, all naturally occurring charged amino acids can be identified as either electron donor (D), bridge (B), or electron acceptor (A) units. Within protein folds, the charged side chains of these amino acids (e.g., Lys amino or Glu carboxyl groups), and the peptide backbone play the role of D and A groups, while the aliphatic (non-polar) part of the side chain or the intervening protein/solvent medium forms the B component of the D−B−A units. While CT transitions for charged amino acid monomers are expected to be in the deep UV (below 250 nm), strong inter-residue electronic couplings imposed by protein folds can shift such transitions dramatically to the visible end. Previous molecular dynamics (MD) and electronic structure analysis revealed three specific factors which primarily determine the ProCharTS absorption range: (1) distance between the side chains of charged amino acids (which could be in the range of 2–10 A or more), (2) the charge complementarity of the interacting side chains and (3) the medium pH [29]. Solvation and conformations of the amino acid side chains and the peptide backbone were also shown to modulate the spectral range of the CT transitions to a lesser extent [28].

Several fast detection assays for coronavirus RNA or proteins have been reported in literature. One of the earliest such assays was based on colorimetric detection of oligonucleotide sequences that bypasses the need for RNA amplification [30]. The assay exploited the electrostatic adsorption of single *versus* double-stranded DNA molecules on gold nanoparticles (NPs). Detection was apparent in about 5 minutes by a change in color due to NP aggregation caused by the hybridization reaction. Although the assay provides fast detection using unmodified commercially available materials, its use of NPs increases the cost of the assay. A dual-functional plasmonic biosensor that uses both localized surface plasmon resonance sensing transduction and the plasmonic photothermal effect showed a detection time of approximately 14 minutes [22]. However, the assay demands surface functionalization and viral sequence detection which requires sophisticated and complex sample preparation and handling. An optical detection assay that uses the principle of fluorescence and detects presence of the nucleocapsid protein of SARS-CoV-2 in urine and nasopharyngeal swabs has been proposed [31]. It comprises immunochromatographic strip with a sample well. A diluted patient specimen is added to the well and after 10 minutes, the strip is loaded into an immunofluorescence analyzer, which automatically determines the results based on a reference fluorescence value determined previously. The challenge of this assay is that it requires a skilled professional to operate the immunofluorescence analyzer. An immunosensor utilizing a sensitive graphene Field Effect Transistor has recently been proposed that can identify and detect the SAR-CoV-2 spike protein in about 2 minutes [32]. Electrical detection of the antibody-antigen interaction is used as the sensing mechanism whereby the slightly positively charged S1 protein hybridizes with the spike S1 subunit protein antibody immobilized on the graphene electrode, affecting its conductance/resistance via field effect. The limitation of this assay is that it requires complex preparation of the electrodes and its effectiveness depends largely on the immobilization of spike S1 subunit protein antibody on the electrodes. Most recently, a rapid, label-free assay based on electrochemical impedance detection in under 5 minutes has been proposed [33]. The assay employs an impedance sensing platform with wells that contain electrodes coated with SARS-CoV-2 receptor binding domain of the spike protein. COVID-19 positive and negative samples are differentiated by the variation in spikes of impedance measurements. Although the assay provides a simple protocol for testing the impedance sensing platform, it is quite costly.

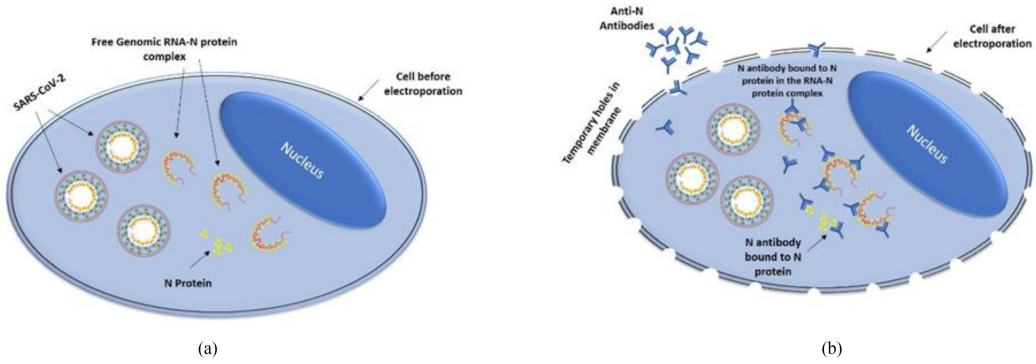

(a) (b)

Fig. 1. Schematic illustration of SARS-CoV-2 N protein with anti-N binding. (a), (b) are the cells without and with electrical biasing, respectively.

Electrostatic analysis has been used previously to study protein interactions at a structural level. For example, it was observed that the protein surface of ACE2 shows negative electrostatic potential, while the S proteins of the SARS-CoV/SARS-CoV-2 exhibit positive potential [34]. Additionally, it was found that SARS-CoV-2 S protein is slightly more positively charged than that of SARS-CoV, giving it a higher affinity to bind to negatively charged regions of the ACE2 (30% higher binding energy [7]). Similarly, the SARS-CoV-2 N protein has three distinct but highly conserved parts: the N-terminal RNA-binding domain (NTD) which is responsible for RNA binding via its distinct basic (positively charged) finger and palm regions: a C-terminal dimerization domain (CTD) which is responsible for oligomerization, and intrinsically disordered central Ser/Arg (SR)-rich linker which is responsible for linker for primary phosphorylation, respectively [35]. Thus, in this study, we exploited the higher positive electrostatic potential of SARS-CoV-2 N protein and its antibody to develop an opto-electrical assay to successfully detect virus infection in nasal swabs from SARS-CoV-2-infected individuals.

II. Study Rationale and Assay Design

It has been shown that antibody to the N protein of SARS-CoV-2 is more sensitive than S protein antibody for detecting early infection [36]. Typically, antibody binding surfaces are largely negatively charged [37]. The N antibody-antigen complex is formed by electrostatic interactions between the positively charged RNA binding site of the N protein and the oppositely charged surfaces of the antibody. Generally, high affinity antibodies as well as the rigid parts of the proteins have higher and stronger electrostatic interactions [38]. Moreover, an antibody can be introduced into the cell by electro-insertion that allows antibodies to penetrate the cell or cell content to be expressed out of the cell. The infected cell physiology with and without the application of electric field is illustrated in Fig. 1(a) and (b), respectively. The cell is assumed to be suspended in the aqueous transport medium of a nasopharyngeal swab along with anti-N antibodies (anti-N). When the electrical pulse is applied, the cell opens up by the formation of pores in the cell membrane. The pores only stay open for the duration of the applied constant field or its time domain variation. The anti-N antibody penetrates the cell through these pores and binds with the N protein of SARS-CoV-2 virus that is expressed during infection [8]. This interaction or binding could be used as a reliable marker for the presence of infection and of virus replication as the protein-antigen binding of the infected cell should create a change in the electric properties of the cell that can be measured. Thus, in this assay, the binding between N protein and anti-N was enabled electrically and detected optically. The optical intensities for the nasal samples with antibodies were measured at zero and one volt with time. The experimental setup utilized in this study is shown in Fig. 2(a), incorporating a mini spectrometer and a smart mobile phone that was employed as a light source with its power spectrum exhibiting maximum power at a wavelength of 623 nm [39]. The mini-spectrometer C11708MA (Hamamatsu/Japan) was used to measure the light intensity as it passed through test samples with spectral response ranging from 590 nm to 1100 nm [40]. The sample under test was placed between the mobile light source and the mini-spectrometer, as shown in Fig. 2(a). The distances between the light source, the spectrometer, and the sample holder were adjusted to eliminate any possible interference and to stabilize the spectrometer performance.

The portable photospectrometer was aligned with the light source and sample cuvette to achieve a straight path of light. The 0.4 cm-gap micropulser electroporation cuvettes from Bio-Rad were used for the electrical analysis [41]. The cuvette incorporates aluminum electrodes plates with an area of 1 cm by 0.8 cm. Its outer dimensions are $12.5 \times 12.5 \times 45$ mm (W $\times$ D $\times$ H) with a path length of 10 mm and a functional volume between 50–1,500 µl. The biasing voltage required was applied using the Gamry 3000 instrument [42].

Fig. 2(b) shows the nasal swab buffer optical light density measurements *versus* wavelength from 590 nm to 1100 nm. The corresponding smart mobile power spectrum is depicted in Fig. 2(c). As can be seen, the maximum optical power was emitted at a wavelength of 623 nm; therefore, this wavelength was chosen for further experimentation. At 623 nm, the sensitivity of the measurements was higher than at any other wavelength, showing the reproducibility of the results. Initial test of this experimental setup revealed that it had one major drawback, that is, when samples were loaded into the cuvette, the angle and position of the cuvette changed which affected the results obtained. To ensure that the results were reproducible, the measurements for the same sample were conducted over different days and on each day, the setup was standardized since

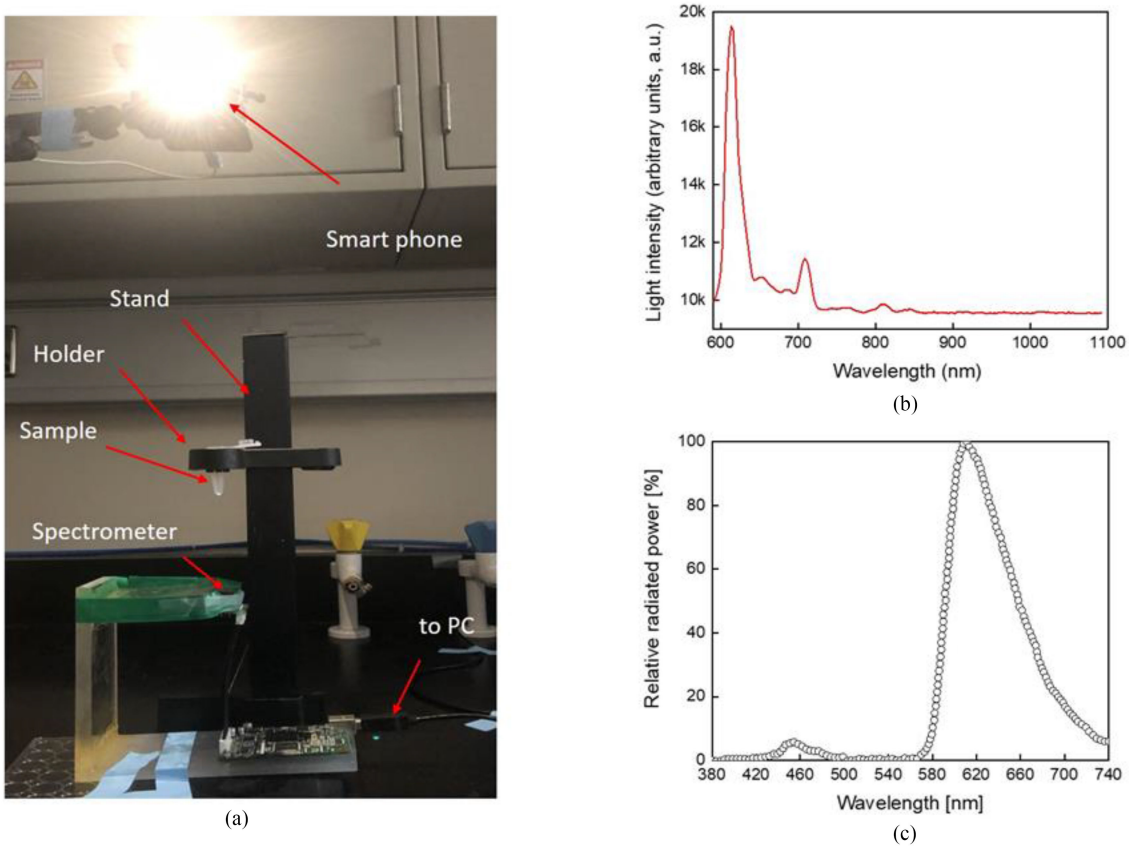

Fig. 2. The proposed concept of optical detection and the experimental design: (a) Optical measurement setup is shown consisting of a smart phone as a light source and the mini-spectrometer utilized to collect the light waves passing through the sample kept in the holder. (b) Light intensity of the buffer of the nasal swab and (c) power intensity of the used smart phone.

the position of the mobile phone, spectrometer and samples could vary. To overcome this caveat and have more consistent measurements without constant standardization, the ability of the spectrometer to provide light intensity measurements over time, was taken advantage of the optico-electrical response in the form of a change in light intensity at different electrical biases was recorded for all tests over time.

To test the proof-of-principle, nasal swab samples from patients with known negative or positive COVID-19 results were tested using our experimental design. The patient results were confirmed using real time RT-qPCR assay. Two specimens of 150 µl each were taken from the nasal swabs suspended in the viral transport media (VTM). The first specimen was left as purely the patient sample, while 150 µl of anti-N antibody with a concentration of 1 μg/mL was added to the second specimen. The samples were loaded in the Bio-Rad cuvettes which were then characterized for their optical properties with time in the absence or presence of one volt of electrical bias using the apparatus described in Fig. 2(a).

III. Results and Analysis

Fig. 3(a) and (b) show the measured optical light intensity *versus* time for these samples either alone or in the presence of anti-N antibody under zero and one volt voltage bias conditions. As can be observed for the individual negative and positive samples in the absence of the anti-N antibody (blue curves), the light intensity exhibited a somewhat linear behavior where it slowly increased with increasing time of observation at zero voltage bias. This trend remained the same at one volt bias for the negative sample (Fig. 3(a)), while the curve became nearly flat for the COVID-19(+) sample in the presence of the one volt bias (Fig. 3(b)). Overall, the behavior of light did not change much between the zero and one volt bias for the negative samples alone. In contrast, the slope of both the COVID-19 negative and positive samples changed noticeably in the presence of the anti-N antibody between the zero and one volt conditions, depicting a stable linear behavior in the downward direction (Fig. 3(a) & (b)). The changes in the sample profiles at one volt bias in the presence of anti-N antibodies are interpreted to reflect the binding between the antibodies and the N proteins in the COVID-19(+) cells. As the binding interactions start, the corresponding optical profiles descend incrementally due to the increase in binding events, releasing more energy photons [43].

The current detection approach starts with normalizing the measured intensities, each to its corresponding y-intercept, to unify the scales and allow determination of the variations clearly. It is worth mentioning that the level of the light intensity was influenced by insertion of the cuvette and its cable connections. Therefore, normalization with respect to the y-intercept levels

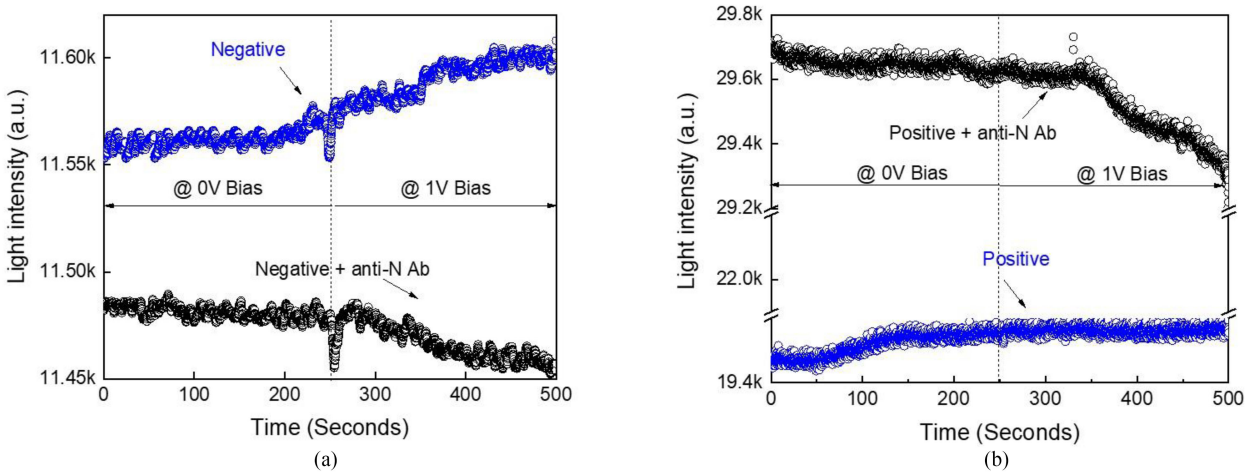

Fig. 3. Measured optical light intensity *versus* time for: (a) a representative COVID-19 negative nasal swab sample alone or in the presence of anti-N antibody (Ab) under zero and one volt DC bias. (b) The measured optical light intensity *versus* time for a representative COVID-19 positive nasal swab sample alone or in the presence of anti-N antibody under zero and one volt bias. The specimen and the antibody volumes were the same at 150 µl each. The anti-N antibody was used for the detection of SARS-CoV-2 N protein which can detect 4 ng of free peptide at a concentration of 1 μg/mL.

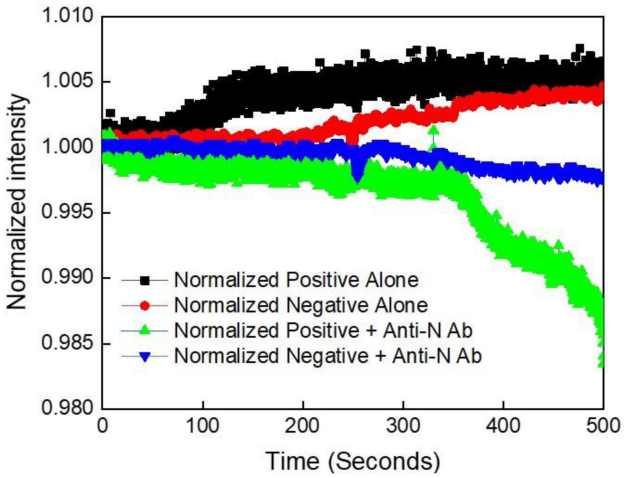

Fig. 4. Normalized measured light intensities *versus* time, each to its corresponding y-intercept.

TABLE I
RATE OF CHANGE IN THE NORMALIZED MEASURED LIGHT INTENSITY OF NASAL SWAB SAMPLES FROM COVID-19 (−) AND TEN COVID (+) SAMPLES EACH

Sample	Slope @ zero	Slope @ 1 V	Variation	Figure of Merit (FOM)
Positive alone	2.25E-06	3.95E-08	2.21E-06	
Negative alone	2.29E-07	1.01E-06	-7.82E-07	
Positive + Anti-N Ab	-6.36E-07	-5.92E-06	5.29E-06	2.07E+00
Negative + Anti-N Ab	-2.02E-07	-9.54E-07	7.51E-07	8.02E-01

helps to overcome this issue. The normalized graphs are shown in Fig. 4. Both negative samples (with and without the anti-N antibodies) exhibited more linear responses than the positive samples. The normalized curves also confirm interactions between antibodies and the coronavirus in the positive sample (see the green curve), which represents the normalized positive sample with anti-N antibodies. The slopes of the entire time intervals before applying bias were measured. The slopes of the negative and positive samples in Fig. 4 were extracted through the process of linear regression during "0" and "1 V" bias. It is recommended to have minimum periods of 100 secs to guarantee that an interaction has occurred that would be reflected in the measured profile. To analyze the behavior of the samples further, the slopes of the corresponding sample normalized profiles were extracted and have been summarized in Table I from ten COVID-19(−) and ten COVID-19(+) individuals.

Fig. 5(a) depicts the relative difference in the measured profile slopes with and without voltage bias. This figure reveals that the absolute extracted slopes for the positive samples in the presence of anti-N antibodies was approximately two times higher than the extracted slopes for the negative samples in the presence of the anti-N antibodies. Therefore, the slope variation above 10% was set as the threshold of detection of a COVID-19 patient with low accuracy.

To have a successful higher accuracy value, the following Figure of Merit (FOM) is proposed:

$$FOM = (SA - S)\,|_{1V} \,/\, (SA - S)\,|_{0V} \tag{1}$$

where SA and S are the samples with antibody and the same sample alone, respectively.

The FOM represents the relative variation of the sample with and without antibody at two different voltages. The corresponding extracted FOM is listed in the last column of Table I. As illustrated in Fig. 5(b), the accuracy of prediction was improved

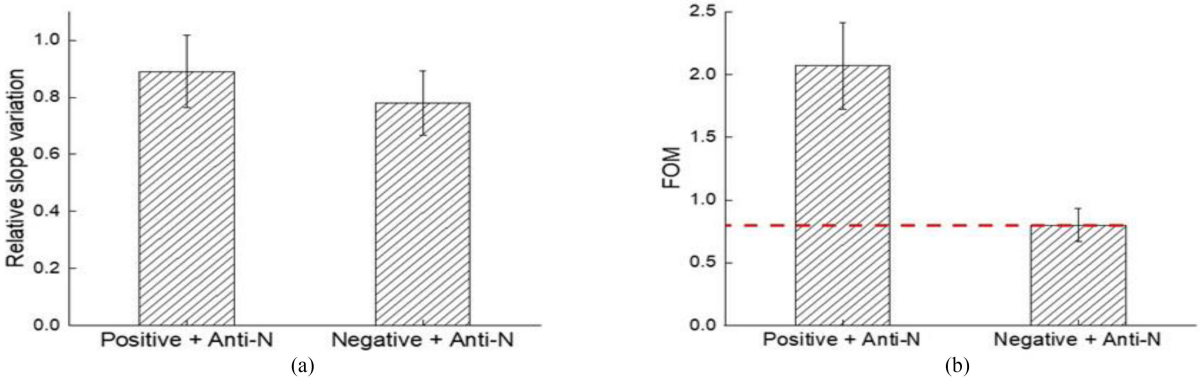

Fig. 5. Analysis of slope variation observed in test samples. (a) The extracted slopes for the negative and positive samples tested in the presence of the anti-N antibody. (b) The extracted Figure of Merit (FOM) of the same samples analyzed as in panel a. The error bars represent the standard deviation from 10 samples from the COVID-19(−) and (+) samples. The red dashed line represents the threshold of successful detection of a negative from a positive COVID-19 sample.

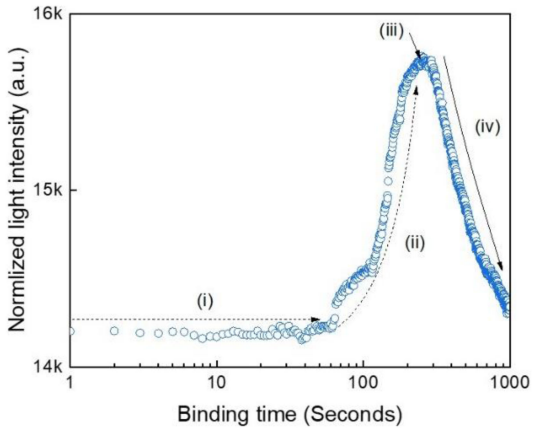

Fig. 6. Measured optical binding profile of N protein with its antibody *versus* time under free binding conditions without the application of any biasing voltage.

dramatically. Based on the results obtained from ten negative and positive nasal swab samples each, an FOM of above 1 should be able to successfully predict the COVID-19 status of a patient with 100% accuracy using this approach. For rapid and quick detection, the nasal swab can be split into four specimens and the four required tests (sample at zero and one volt, sample with anti-N Ab at zero and one volts) can be run simultaneously to collect the corresponding optical profiles for 100 seconds. The data can then be processed to extract the slopes and the FOM to have the results.

A. Assay Validation

To validate our results that the molecular interactions being observed by the opto-electrical was really detecting SARS-CoV-2-antibody interactions in nasal swab samples, we conducted the following experiment. The binding behavior of a solution of SARS-CoV-2 N protein in the presence of its antibody was analyzed under visible light in the range of 623 nm in a test tube. Fig. 6 shows the measured binding profile of the N protein with its antibody *versus* time under free binding conditions without the application of any biasing voltage. As can be seen, a nice "hump" was observed (as an increase in arbitrary units (a.u.) with time) which is a direct indication of the binding reaction occurring at 623 nm wavelength. Based on these observations, we believe that a "hump or spike" in light intensity is observed when a specific molecular interaction takes place between two proteins. This is mainly due to the physio-chemical properties of the proteins that relates to binding affinity in the contact surface area and incorporates the association/dissociation process [44]. As revealed from the corresponding binding measured light intensity profiles, such interactions exhibit Gaussian-like peaks. Wang *et al.* have demonstrated that molecular binding at a single molecule level displays such a peak [45]. Interestingly, Kozono *et al.* monitored the real-time Brownian motion and fitted it with Gaussian function [46]. The fitting parameters of the distributions can provide many features of the binding interactions [47]. This could provide a quantitative signature or characterization of a specific antigen binding to a specific antibody such as intrinsic specificity and binding rate. It has also been shown that the probability of the binding free energy has a Gaussian distribution near the mean and exponential-like distribution in the tail [48]. As described in Fig. 6, the time slot denoted by (i) represents the time just before the interaction occurs. As the interaction starts, the corresponding optical profile ascends incrementally as indicated by (ii) due to the increase in binding events which affect the protein folding and increase the CT transitions, releasing more energy photon. The peak pointed by (iii) occurs at the maximum event of binding between the antigen and the antibody. The height of the peak indicates stronger interactions and *vice versa*. The profile then descends till the end as the binding events becomes less and no further interactions occur at the end, as illustrated by (iv). The distance in time to maximum peak reflects the speed of the binding interactions; thus, the earlier the peak appears, the faster the binding interaction takes place.

B. Determination of Applied DC Pulse

To study the effect of DC biasing on a protein solution, the anti-N antibody was suspended in a buffer and loaded in an electroporation cuvette that incorporates two electrodes with a volume of 0.5 mL and a separation distance of 0.4 cm. The

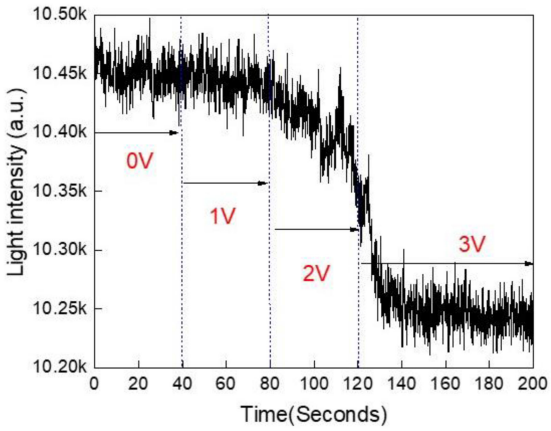

Fig. 7. Measured anti-N antibody optical response *versus* time at different DC bias voltages.

optical response *versus* time at different DC bias voltages was recorded and depicted in Fig. 7. As can be seen, Fig. 7 reveals that the optical response decayed slowly with the application of DC bias between 0 and 2V. However, by 3 volts DC bias, the optical response dropped with a considerable step and we believe that increasing the DC bias further essentially burns the suspension and destroys it. Thus, an applied bias should result in induction of a current across the suspension and if this current is high enough, it should have the potential to destroy the protein physiology and functionality, resulting in the loss of specific protein-protein interactions. Therefore, we conclude that 1V DC bias was an optimum value that promoted the entry of the anti-N antibody into cells without changing the configuration and physiology of the viral nucleocapsid protein, the cells, buffer, or antibodies.

IV. Discussion

In comparison to these expensive and cumbersome assays discussed in the literature review, our study provides proof-of-concept for an opto-electrical assay used to detect SARS-CoV-2 in patient nasal swab samples by combining measured optical light intensity under the application of electrical bias within 2 minutes. The principle was established by testing protein-protein interactions of both positive and negative patient samples individually, as well as in combination with anti-N antibody under 0V and 1V serially applied bias voltages. The applied bias voltage was limited to 1V voltage bias because beyond about 3V DC, the electric field becomes too intense for the cells to recover their membrane and cell functions [49]. The electroporated antibody and intracellular N antigen bind and their binding interactions can then be optically detected as a change in the light intensity measured by the mini photo spectrometer. For the pure samples (the negative only and positive only samples, respectively), the light intensity increased on application of the 1V bias voltage. The extraction of FOM removed any systematic errors, background noise and discrepancies due to system calibration. It also provided a clearer picture of the analyte response for comparison. We further verified that the change in light intensity was mainly due to change in protein folding that occurs inside the cell as a result of applying 1V to allow them to enter the cell. These changes reflect alterations in hydrogen bonding and charge transfer between amino acid charged side chains and the polypeptide backbone due to the interaction of the N antibody with N proteins These results are in line with previous studies which have shown that addition/electro-insertion of an antibody into a cell that selectively binds to a protein can be used as a means to distinguish the electrical signature of analytes [23], [50].

Thus, our assay is based on the principle that the aggregation of protein chains containing both secondary and tertiary structure of protein upon N protein interaction with its antibodies could allow CT transitions as illustrated in Fig. 8. Fig. 8(a) shows the SARS-CoV-2 nucleocapsid proteins approaching anti-N antibodies. Fig. 8(b), shows the two proteins getting closer to each other and as they do that, some changes in the proteins 2D and 3 D structure are initiated due to electrostatic interactions between charged side chains and/or hydrogen bonding and other intermolecular forces. Fig. 8(c) shows the binding between the two proteins through electrostatic interactions, H-bonding and other intermolecular forces; upon light irradiation, charge transfer transitions between amino acids with charged side chains and polypeptide backbone take place. This is illustrated more clearly in Fig. 8(d), which shows charge transfer transitions between the charged side groups of amino acids, Arg and Asp as examples, and the polypeptide backbone. These charge transfer transitions are thought to occur between electronic donor amino acids in the interacting proteins with charged side chains and electron acceptors amino acids upon UV-Vis irradiation. While CT transitions for charged amino acid monomers are expected to be in the deep UV (below 250 nm) range, strong inter-residue electronic couplings imposed by protein folds can shift such transitions dramatically to the visible range [25], [27]. The photoelectric effect theory combines kinetic, binding and photon energies, all three of which are correlated through the theoretical physics fundamentals and principles [51]. Hence, if the generated photon energy due to the binding interactions is sufficient, it could give rise to light intensity at a specific wavelength [43]. Wang *et al.* have discussed the enhancement of receptor binding of SARS-CoV-2 through networks of hydrogen-bonding and hydrophobic interactions [52]. They have provided explanations to better understand the structural and energetic details responsible for protein–protein interactions. Their simulations reveal that both electrostatic complementarity and hydrophobic interactions are critical to enhance receptor binding and escape antibody recognition by the receptor binding domain (RBD) of SARS-CoV-2. Furthermore, Dahal *et al.* have demonstrated that binding probability increases with antibody concentration and the stability of protein [53]. Grisanti *et al.* relate the optical properties of the folded proteins to electron driven proton transfer along hydrogen bonds in γ and β protein turns [54]. Charged amino acids such as Lys, Arg, His and Glu that are integral constituents of DNA and RNA binding proteins, glycoproteins and estrogen binding proteins, respectively, have been found to possess unique characteristic absorption features extending beyond 320 nm due to charge transfer transitions involving the amino ($-NH_3^+$) and carboxyl ($-COO^-$) groups of their side chains and the polypeptide backbone [28].

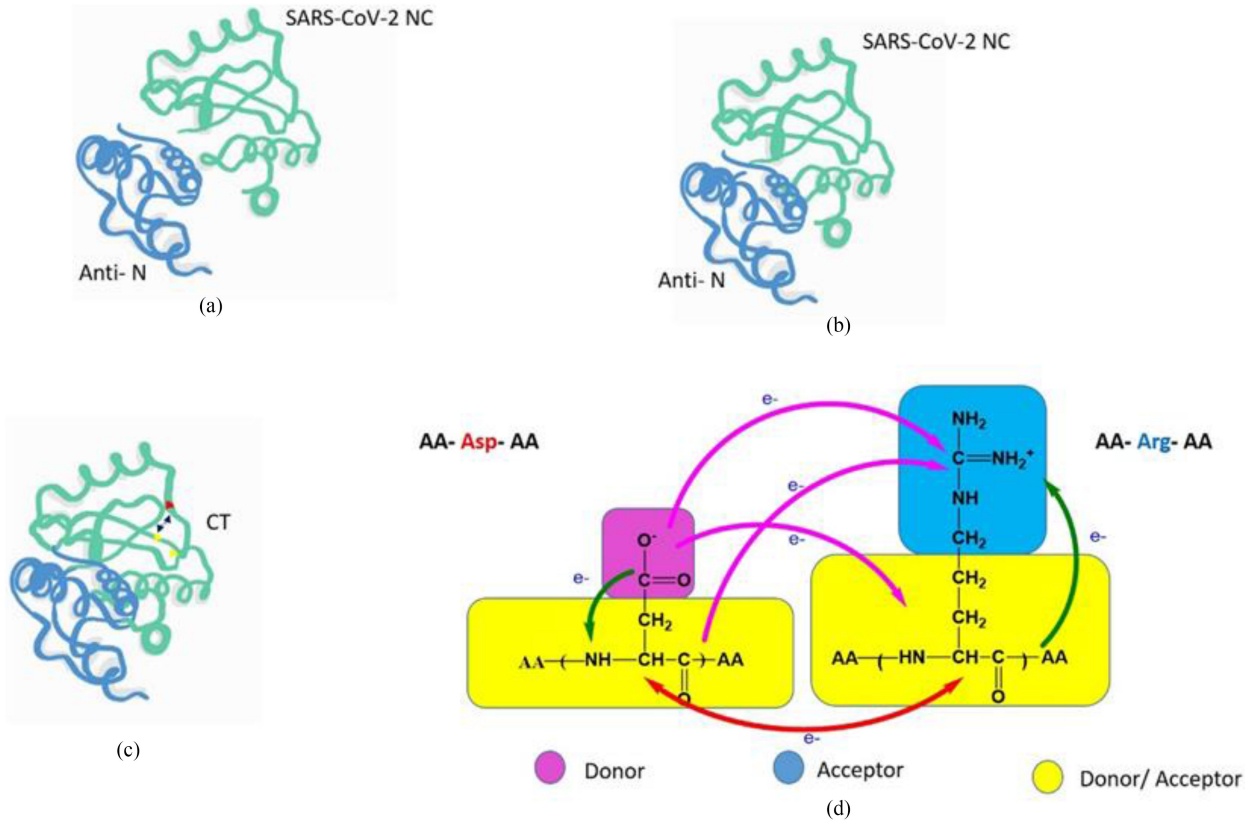

Fig. 8. Illustration of protein charge transfer transitions that take place between SARS-CoV-2 nucleocapsid protein and anti-N antibodies. Panel (a) shows the two proteins apart, (b) shows the two proteins getting closer, and (c) shows the binding between the two proteins through hydrogen bonding and other intermolecular forces. Panel (d) Illustration of how upon light irradiation, charge transfer transitions between amino acids with charged side chains and polypeptide backbone takes place.

The performance of diagnostic tests can be gauged depending upon a number of metrics. Commonly used are sensitivity and specificity. Sensitivity refers to the ability of the test in question to correctly identify the proportion of samples that are genuinely positive, such as detecting a disease, whereas specificity refers to the ability of the test in question to correctly identify the proportion of samples that are truly negative such as patients that do not have the disease. The World Health Organization (WHO) recommends a minimum of 80% sensitivity and 97% specificity for the rapid antigen test [55]. The proposed opto-electrical method exhibited a sensitivity of 90.91% and a specificity of 90.91%. These results are based on comparison of our results with the clinically-validated real time RT-qPCR test that was used for clinical detection of SARS-CoV-2 initially.

Our proposed assay is compared with other detection assays/instruments from a number of perspectives, including need for sample preparation, test duration, operational difficulties, and other factors [14], [17], [21], [22], [56]–[65] as shown in Table II.

The opto-electrical assay described in this study can be practically functionalized by creating a compact sensing and control unit linked to a smart phone mobile application, making it portable and highly efficient. The unit will comprise a custom-built, electrode-embedded well that will act as the sample holder and sensing element. The patient sample (VTM from the nasopharyngeal swab) and N protein antibody solution will be added to the well via a teardrop pipette. Once light from a smart phone camera is incident on the well, the electrode will deliver up to 1V voltage bias to the solution under test. The microelectronic circuitry within the unit will processes the signal transduced by the sensor and communicate the data wirelessly via Bluetooth or any other suitable wireless protocol to the mobile application installed on the smart phone. To allow for portability, the sensing unit will have an inbuilt battery that can be charged using a power cable connected to a power charging port. The calculated cost of such a test would be less than $3, which is the cheapest ever one can have compared to existing tests. This approach can be further developed to accommodate mass screening that should provide fast and accurate positive or negative test results in the field without the need for any sample processing or analysis. If the results are positive, the results could be validated by the more conventional techniques for further verification.

V. Conclusion

A novel proof-of-concept biosensor for the detection of SARS-CoV-2 is presented. The detection method utilizes electroporation and opto-electrical detection of viral nucleocapsid protein and anti-N antibody interactions. A FOM was derived

TABLE II
COMPARISON OF PROPOSED ASSAY WITH OTHER DETECTION TECHNIQUES IN THE LITERATURE

Detection System	RT-PCR [56][57] [59-61][65]	CRISPR [56-58] [59][17]	RT-LAMP [57][58][60] [62][65]	Rapid Antigen [57][63-65]	Nano RT-PCR [14]	FET Biosensor [21]	Plasmonic Biosensor [22]	This Work
Sample preparation	Yes	Yes	Yes	No	Yes	No	Yes	No
Molecule tested	mRNA	mRNA	mRNA	Antigen	mRNA	Antigen	mRNA	Antigen
Test duration	Hours to day(s), depending upon system	15-60 min	15-60 min	15-30 min	17 min	-	-	2 min
Operation functionality	Complex	Complex	Complex	Medium	Complex	Complex	Complex	Simple
Sensitivity (%)	90-100	95-100	98.7-100	91.4-97.6	>80%	-	-	90.91%
Specificity (%)	100	100	96.1-100	98.08-100	>97%	-	-	90.91%
Test cost	Medium	Low	Medium	Low	High	-	-	Low
System cost	High	Low	Medium	-	-	-	-	Low
Environ. impact*	High	High	High	Low	Low	-	-	Low
Portability	No	Yes	No	Yes	Yes	No	No	Yes
Equipment Footprint	Large	Large	Medium	Small	Small	Small	Small	Small
Data connectivity	NA	Yes	NA	Yes	NA	NA	NA	Yes
Battery operated	No	Yes	No	NA	Yes	No	No	Yes

*Determined by the amount of plastic material, gloves, gowns and other personal protection equipment (PPE) and biomedical waste per test.

that allows for clear distinction between positive and negative nasal swab samples with a threshold value >1 indicating a positive sample and a threshold value <1 indicating a negative value, respectively. The assay uses simple instrumentation that allows for scaling, either for portability or for mass screening. It provides an easy to implement, label-free and low cost diagnostic platform for early detection of COVID-19 within two minutes.

APPENDIX

A. Optical Mini-Spectrometers

Optical Mini-Spectrometers C11708MA from Hamamatsu/Japan [40] was used to convert the variable attenuation of light waves as they passed from end-to-end or reflect off substances into signals with spectral response ranging from 640 to 1010 nm. The wavelength reproducibility ranged between -0.5 to 0.5 nm and had a maximum of 20 nm FWHM spectra, under constant light conditions. The measurements were conducted with the room lights on. The distance between the light source, the spectrometer, and the sample holder were adjusted to eliminate any possible interference and to stabilize the spectrometer performance. Furthermore, the spectrometer was aligned with the light source and sample cuvette to achieve a straight path of light.

B. Light Source

A smartphone light source was used as the main light source. The mobile light emits light with the spectral range from 380 to 740 nm. The maximum optical power was emitted at a wavelength of 623 nm [39]. In this work, iPhone 8 was employed, though any smart phone can be used [66].

C. Electroporation Cuvette

The MicroPulser Electroporation Cuvettes (0.4 cm-gap) from Bio-Rad were used for the electrical analysis [67]. This a high-quality cuvette which is compatible with most electroporation systems. The cuvette incorporates aluminum electrodes plates with an area of 1 cm by 0.8 cm. Its outer dimensions are 12.5 x 12.5 x 45 mm (W x D x H) with a path length of 10 mm and a functional volume between 50–1,500 µl.

D. Gamry Reference 3000™

It is a high-performance electrical analyzer that was used to apply the biasing voltage required in this work [42]. The Gamry analyzer exhibits a high-current, high-performance potentiostat, fully equipped to perform impedance spectroscopy up to 1 MHz.

E. Patient Samples

Ten selected positive and 10 negative patient samples were used for this study. They were extracted from the upper respiratory tract by nasopharyngeal swabs suspended in viral transport media (VTM). The specimen were confirmed clinically for their virus status by the Al Ain Hospital, Al Ain using real-time RT-qPCR identification of SARS-CoV-2 RNA, following all relevant guidelines and regulations (cobas 6800, P/N 09175431190). All procedures were given ethical approval by the Abu Dhabi Department of Health reference DOH/CVDC/2020/872 issued on May 6, 2020.

F. SARS-CoV-2 Nucleocapsid Antibody

SARS-CoV-2 nucleocapsid antibody (rabbit polyclonal anti-N antibody at a stock concentration of 1 mg/ml) from (Sino Biologicals Cat no. 40588-T62) [68] was used for the affinity binding experiments. The lyophilized protein was resuspended at a stock concentration of 0.25 mg/ml according to the manufacturer's instruction in sterile water.

G. SARS-CoV-2 Nucleocapsid Protein

SARS-CoV-2 nucleocapsid protein from (Sino Biologicals, Cat no. 40588-V08B) [68] was used for the binding affinity experiments. The lyophilized protein was resuspended at a stock concentration of 0.25 mg/ml according to the manufacturer's instruction in sterile water.

ACKNOWLEDGMENT

The authors appreciate the assistance received from Abu Dhabi Department of Health as well as the continuous help and support received from the UAEU Research office at UAEU.

REFERENCES

[1] F. Wu *et al.*, "A new coronavirus associated with human respiratory disease in China," *Nature*, vol. 579, no. 7798, pp. 265–269, Mar. 2020, doi: 10.1038/s41586-020-2008-3.

[2] Center for Systems Science and Engineering, "COVID-19 dashboard by the Center for Systems Science and Engineering (CSSE) at Johns Hopkins University (JHU)," John Hopkins Univ., 2020. Accessed: Dec. 23, 2021. [Online]. Available: https://coronavirus.jhu.edu/map.html

[3] J. Lan *et al.*, "Structure of the SARS-CoV-2 spike receptor-binding domain bound to the ACE2 receptor," *Nature*, vol. 581, no. 7807, pp. 215–220, May 2020, doi: 10.1038/s41586-020-2180-5.

[4] R. Yan, Y. Zhang, Y. Li, L. Xia, Y. Guo, and Q. Zhou, "Structural basis for the recognition of SARS-CoV-2 by full-length human ACE2," *Science (80-.)*, vol. 367, no. 6485, pp. 1444–1448, Mar. 2020, doi: 10.1126/science.abb2762.

[5] X. Ou *et al.*, "Characterization of spike glycoprotein of SARS-CoV-2 on virus entry and its immune cross-reactivity with SARS-CoV," *Nat. Commun.*, vol. 11, no. 1, Dec. 2020, Art. no. 1620, doi: 10.1038/s41467-020-15562-9.

[6] Y. Chen, Q. Liu, and D. Guo, "Emerging coronaviruses: Genome structure, replication, and pathogenesis," *J. Med. Virol.*, vol. 92, no. 4, pp. 418–423, Apr. 2020, doi: 10.1002/jmv.25681.

[7] K. Hassanzadeh *et al.*, "Considerations around the SARS-CoV-2 spike protein with particular attention to COVID-19 brain infection and neurological symptoms," *ACS Chem. Neurosci.*, vol. 11, no. 15, pp. 2361–2369, Aug. 2020, doi: 10.1021/acschemneuro.0c00373.

[8] Y. Cong *et al.*, "Nucleocapsid protein recruitment to replication-transcription complexes plays a crucial role in coronaviral life cycle," *J. Virol.*, vol. 94, no. 4, Nov. 2019, Art. no. e01925-19, doi: 10.1128/JVI.01925-19.

[9] H. Jamshaid *et al.*, "Diagnostic and treatment strategies for COVID-19," *AAPS PharmSciTech*, vol. 21, no. 6, pp. 222–236, Aug. 2020, doi: 10.1208/s12249-020-01756-3.

[10] L. J. Carter *et al.*, "Assay techniques and test development for COVID-19 diagnosis," *ACS Cent. Sci.*, vol. 6, no. 5, pp. 591–605, May 2020, doi: 10.1021/acscentsci.0c00501.

[11] P. Pokhrel, C. Hu, and H. Mao, "Detecting the coronavirus (COVID-19)," *ACS Sensors*, vol. 5, no. 8, pp. 2283–2296, Aug. 2020, doi: 10.1021/acssensors.0c01153.

[12] O. Vandenberg, D. Martiny, O. Rochas, A. van Belkum, and Z. Kozlakidis, "Considerations for diagnostic COVID-19 tests," *Nat. Rev. Microbiol.*, vol. 19, pp. 171–183, 2021, doi: 10.1038/s41579-020-00461-z.

[13] A. Ganguli *et al.*, "Rapid isothermal amplification and portable detection system for SARS-CoV-2," *Proc. Nat. Acad. Sci.*, vol. 117, no. 37, pp. 22727–22735, Sep. 2020, doi: 10.1073/pnas.2014739117.

[14] J. Cheong *et al.*, "Fast detection of SARS-CoV-2 RNA via the integration of plasmonic thermocycling and fluorescence detection in a portable device," *Nat. Biomed. Eng.*, vol. 4, no. 12, pp. 1159–1167, Dec. 2020, doi: 10.1038/s41551-020-00654-0.

[15] F. Palaz, A. K. Kalkan, A. Tozluyurt, and M. Ozsoz, "CRISPR-based tools: Alternative methods for the diagnosis of COVID-19," *Clin. Biochem.*, vol. 89, pp. 1–13, Mar. 2021, doi: 10.1016/j.clinbiochem.2020.12.011.

[16] "CRISPR-based portable COVID tests," *Nat. Biotechnol.*, vol. 39, no. 9, pp. 1031–1031, Sep. 2021, doi: 10.1038/s41587-021-01061-9.

[17] H. de Puig *et al.*, "Minimally instrumented SHERLOCK (miSHERLOCK) for CRISPR-based point-of-care diagnosis of SARS-CoV-2 and emerging variants," *Sci. Adv.*, vol. 7, no. 32, Aug. 2021, Art. no. eabh2944, doi: 10.1126/sciadv.abh2944.

[18] T. Y. Liu *et al.*, "Accelerated RNA detection using tandem CRISPR nucleases," *Nat. Chem. Biol.*, vol. 17, no. 9, pp. 982–988, Sep. 2021, doi: 10.1038/s41589-021-00842-2.

[19] R. Samson, G. R. Navale, and M. S. Dharne, "Biosensors: Frontiers in rapid detection of COVID-19," *3 Biotech*, vol. 10, no. 9, pp. 385–394, Sep. 2020, doi: 10.1007/s13205-020-02369-0.

[20] E. Sheikhzadeh, S. Eissa, A. Ismail, and M. Zourob, "Diagnostic techniques for COVID-19 and new developments," *Talanta*, vol. 220, Dec. 2020, Art. no. 121392, doi: 10.1016/j.talanta.2020.121392.

[21] G. Seo *et al.*, "Rapid detection of COVID-19 causative virus (SARS-CoV-2) in human nasopharyngeal swab specimens using field-effect transistor-based biosensor," *ACS Nano*, vol. 14, no. 4, pp. 5135–5142, Apr. 2020, doi: 10.1021/acsnano.0c02823.

[22] G. Qiu, Z. Gai, Y. Tao, J. Schmitt, G. A. Kullak-Ublick, and J. Wang, "Dual-functional plasmonic photothermal biosensors for highly accurate severe acute respiratory syndrome coronavirus 2 detection," *ACS Nano*, vol. 14, no. 5, pp. 5268–5277, 2020, doi: 10.1021/acsnano.0c02439.

[23] S. Mavrikou, G. Moschopoulou, V. Tsekouras, and S. Kintzios, "Development of a portable, ultra-rapid and ultra-sensitive cell-based biosensor for the direct detection of the SARS-CoV-2 S1 spike protein antigen," *Sensors*, vol. 20, no. 11, May 2020, Art. no. 3121, doi: 10.3390/s20113121.

[24] T. J. Park, M. S. Hyun, H. J. Lee, S. Y. Lee, and S. Ko, "A self-assembled fusion protein-based surface plasmon resonance biosensor for rapid diagnosis of severe acute respiratory syndrome," *Talanta*, vol. 79, no. 2, pp. 295–301, Jul. 2009, doi: 10.1016/j.talanta.2009.03.051.

[25] I. Mandal, S. Manna, and R. Venkatramani, "UV–Visible Lysine–Glutamate dimer excitations in protein charge transfer spectra: TDDFT descriptions using an optimally tuned CAM-B3LYP functional," *J. Phys. Chem. B*, vol. 123, no. 51, pp. 10967–10979, Dec. 2019, doi: 10.1021/acs.jpcb.9b07827.

[26] M. Z. Ansari *et al.*, "Protein charge transfer absorption spectra: An intrinsic probe to monitor structural and oligomeric transitions in proteins," *Faraday Discuss. J.*, vol. 207, no. 1, pp. 91–113, Feb. 2018, doi: 10.1039/C7FD00194k.

[27] I. Mandal, S. Paul, and R. Venkatramani, "Optical backbone-sidechain charge transfer transitions in proteins sensitive to secondary structure and modifications," *Faraday Discuss,* vol. 207, pp. 115–135, 2018, doi: 10.1039/C7FD00203C.

[28] S. Prasad *et al.*, "Near UV-Visible electronic absorption originating from charged amino acids in a monomeric protein," *Chem. Sci.*, vol. 8, no. 8, pp. 5416–5433, 2017, doi: 10.1039/C7SC00880E.

[29] M. Z. Ansari and R. Swaminathan, "Structure and dynamics at N- and C-terminal regions of intrinsically disordered human c-Myc PEST degron reveal a pH-induced transition," *Proteins Struct. Funct. Bioinform.*, vol. 88, pp. 889–909, 2020, doi: 10.1002/prot.25880.

[30] H. Li and L. Rothberg, "Colorimetric detection of DNA sequences based on electrostatic interactions with unmodified gold nanoparticles," *Proc. Nat. Acad. Sci.*, vol. 101, no. 39, pp. 14036–14039, Sep. 2004, doi: 10.1073/pnas.0406115101.

[31] B. Diao *et al.*, "Diagnosis of acute respiratory syndrome coronavirus 2 infection by detection of nucleocapsid protein," *medRxiv*, 2020, doi: 10.1101/2020.03.07.20032524.

[32] X. Zhang *et al.*, "Electrical probing of COVID-19 spike protein receptor binding domain via a graphene field-effect transistor," Mar. 2020. [Online]. Available: http://arxiv.org/abs/2003.12529

[33] M. Z. Rashed *et al.*, "Rapid detection of SARS-CoV-2 antibodies using electrochemical impedance-based detector," *Biosensors Bioelectron.*, vol. 171, Jan. 2021, Art. no. 112709, doi: 10.1016/j.bios.2020.112709.

[34] S. P. Morton and J. L. Phillips, "Electrostatic characteristics of SARS-CoV-2 spike and human ACE2 protein variations predict mutable binding efficacy," *bioRxiv*, 2020.

[35] S. Kang *et al.*, "Crystal structure of SARS-CoV-2 nucleocapsid protein RNA binding domain reveals potential unique drug targeting sites," *Acta Pharmaceutica Sinica B*, vol. 10, no. 7, pp. 1228–1238, Jul. 2020, doi: 10.1016/j.apsb.2020.04.009.

[36] P. D. Burbelo *et al.*, "Detection of nucleocapsid antibody to SARS-CoV-2 is more sensitive than antibody to spike protein in COVID-19 patients," *medRxiv*, Apr. 2020, doi: 10.1101/2020.04.20.20071423.

[37] M. Wang, D. Zhu, J. Zhu, R. Nussinov, and B. Ma, "Local and global anatomy of antibody-protein antigen recognition," *J. Mol. Recognit.*, vol. 31, no. 5, May 2018, Art. no. e2693, doi: 10.1002/jmr.2693.

[38] N. Sinha and S. Smith-Gill, "Electrostatics in protein binding and function," *Curr. Protein Peptide Sci.*, vol. 3, no. 6, pp. 601–614, Dec. 2002, doi: 10.2174/1389203023380431.

[39] H. Kim, Y. Jung, I.-J. Doh, R. A. Lozano-Mahecha, B. Applegate, and E. Bae, "Smartphone-based low light detection for bioluminescence application," *Sci. Rep.*, vol. 7, no. 1, Feb. 2017, Art. no. 40203, doi: 10.1038/srep40203.

[40] HAMAMATSU, "Mini-spectrometer MS series C11708MA," Datasheet, 2019. [Online]. Available: [Online]. Available: https://www.hamamatsu.com/jp/en/product/type/C11708MA/index.html

[41] H. L. Nguyen, P. D. Lan, N. Q. Thai, D. A. Nissley, E. P. O'Brien, and M. S. Li, "Does SARS-CoV-2 bind to human ACE2 more strongly than does SARS-CoV?," *J. Phys. Chem. B*, vol. 124, no. 34, pp. 7336–7347, Aug. 2020, doi: 10.1021/acs.jpcb.0c04511.

[42] "Gamry instruments." Accessed: Dec. 27, 2021. [Online]. Available: https://www.gamry.com/

[43] A. P. French and E. F. Taylor, *An Introduction to Quantum Physics (M.I.T. Introductory Physics Series)*, 1st ed. Boca Raton, FL, USA: CRC Press, 1979.

[44] P. L. Kastritis and A. M. J. J. Bonvin, "On the binding affinity of macromolecular interactions: Daring to ask why proteins interact," *J. R. Soc. Interface*, vol. 10, no. 79, Feb. 2013, Art. no. 20120835, doi: 10.1098/rsif.2012.0835.

[45] H. Wang, Z. Tang, Y. Wang, G. Ma, and N. Tao, "Probing single molecule binding and free energy profile with plasmonic imaging of nanoparticles," *J. Amer. Chem. Soc.*, vol. 141, no. 40, pp. 16071–16078, Oct. 2019, doi: 10.1021/jacs.9b08405.

[46] H. Kozono *et al.*, "Single-Molecule motions of MHC class II rely on bound peptides," *Biophys. J.*, vol. 108, no. 2, pp. 350–359, Jan. 2015, doi: 10.1016/j.bpj.2014.12.004.

[47] X. Zheng and J. Wang, "The universal statistical distributions of the affinity, equilibrium constants, kinetics and specificity in biomolecular recognition," *PLOS Comput. Biol.*, vol. 11, no. 4, Apr. 2015, Art. no. e1004212, doi: 10.1371/journal.pcbi.1004212.

[48] X. Zheng and J. Wang, "Universal statistical fluctuations in thermodynamics and kinetics of single molecular recognition," *Phys. Chem. Chem. Phys.*, vol. 18, no. 12, pp. 8570–8578, 2016, doi: 10.1039/C5CP06416C.

[49] T. B. Napotnik and D. Miklavčič, "In vitro electroporation detection methods – An overview," *Bioelectrochemistry*, vol. 120, pp. 166–182, Apr. 2018, doi: 10.1016/j.bioelechem.2017.12.005.

[50] L. T. Sexton, L. P. Horne, S. A. Sherrill, G. W. Bishop, L. A. Baker, and C. R. Martin, "Resistive-Pulse studies of proteins and protein/antibody complexes using a conical nanotube sensor," *J. Amer. Chem. Soc.*, vol. 129, no. 43, pp. 13144–13152, Oct. 2007, doi: 10.1021/ja0739943.

[51] B. R. Masters, "Albert Einstein and the nature of light," *Opt. Photon. News*, vol. 23, no. 7, pp. 42–47, Jul. 2012, doi: 10.1364/OPN.23.7.000042.

[52] Y. Wang, M. Liu, and J. Gao, "Enhanced receptor binding of SARS-CoV-2 through networks of hydrogen-bonding and hydrophobic interactions," *Proc. Nat. Acad. Sci. USA*, vol. 117, pp. 13967–13974, 2020, doi: 10.1073/pnas.2008209117.

[53] N. Dahal, J. Nowitzke, A. Eis, and I. Popa, "Binding-Induced stabilization measured on the same molecular protein substrate using single-molecule magnetic tweezers and heterocovalent attachments," *J. Phys. Chem. B*, vol. 124, no. 16, pp. 3283–3290, Apr. 2020, doi: 10.1021/acs.jpcb.0c00167.

[54] L. Grisanti, M. Sapunar, A. Hassanali, and N. Došlić, "Toward understanding optical properties of amyloids: A reaction path and nonadiabatic dynamics study," *J. Amer. Chem. Soc.*, vol. 142, no. 42, pp. 18042–18049, Oct. 2020, doi: 10.1021/jacs.0c07134.

[55] World Health Organization, "SARS-CoV-2 antigen-detecting rapid diagnostic tests: An implementation guide," 2020. [Online]. Available: https://www.who.int/publications/i/item/9789240017740

[56] M. Shen *et al.*, "Recent advances and perspectives of nucleic acid detection for coronavirus," *J. Pharm. Anal.*, vol. 10, no. 2, pp. 97–101, Apr. 2020, doi: 10.1016/j.jpha.2020.02.010.

[57] W. Leber, O. Lammel, A. Siebenhofer, M. Redlberger-Fritz, J. Panovska-Griffiths, and T. Czypionka, "Comparing the diagnostic accuracy of point-of-care lateral flow antigen testing for SARS-CoV-2 with RT-PCR in primary care (REAP-2)," *EClinicalMedicine*, vol. 38, Aug. 2021, Art. no. 101011, doi: 10.1016/j.eclinm.2021.101011.

[58] U.S. Food & Drug Administration, "EUA authorized serology test performanc." Accessed: Oct. 7, 2021. [Online]. Available: https://www.fda.gov/medical-devices/coronavirus-disease-2019-covid-19-emergency-use-authorizations-medical-devices/eua-authorized-serology-test-performance

[59] University of Oxford Center for Evidence-Based Medicine, "What tests could potentially be used for the screening, diagnosis and monitoring of COVID-19 and what are their advantages and disadvantages?" Accessed: Oct. 7, 2021. [Online]. Available: https://www.cebm.net/covid-19/what-tests-could-potentially-be-used-for-the-screening-diagnosis-and-monitoring-of-covid-19-and-what-are-their-advantages-and-disadvantages/

[60] N. Verma, D. Patel, and A. Pandya, "Emerging diagnostic tools for detection of COVID-19 and perspective," *Biomed. Microdevices*, vol. 22, no. 4, pp. 83–101, Dec. 2020, doi: 10.1007/s10544-020-00534-z.

[61] Johns Hopkins Center for Health Security, "COVID-19 testing toolkit." Accessed: Oct. 7, 2021. [Online]. Available: https://www.centerforhealthsecurity.org/covid-19TestingToolkit/testing-basics/types-of-COVID-19-tests/antigen-and-molecular-tests.html

[62] A. Qasem, A. M. Shaw, E. Elkamel, and S. A. Naser, "Coronavirus disease 2019 (COVID-19) diagnostic tools: A focus on detection technologies and limitations," *Curr. Issues Mol. Biol.*, vol. 43, no. 2, pp. 728–748, Jul. 2021, doi: 10.3390/cimb43020053.

[63] B. Giri, S. Pandey, R. Shrestha, K. Pokharel, F. S. Ligler, and B. B. Neupane, "Review of analytical performance of COVID-19 detection methods," *Anal. Bioanal. Chem.*, vol. 413, no. 1, pp. 35–48, Jan. 2021, doi: 10.1007/s00216-020-02889-x.

[64] B. Udugama *et al.*, "Diagnosing COVID-19: The disease and tools for detection," *ACS Nano*, vol. 14, no. 4, pp. 3822–3835, Apr. 2020, doi: 10.1021/acsnano.0c02624.

[65] J. E. Celis, W. Espejo, E. Paredes-Osses, S. A. Contreras, G. Chiang, and P. Bahamonde, "Plastic residues produced with confirmatory testing for COVID-19: Classification, quantification, fate, and impacts on human health," *Sci. Total Environ.*, vol. 760, Mar. 2021, Art. no. 144167, doi: 10.1016/j.scitotenv.2020.144167.

[66] Apple, "Iphone." Accessed: Jun. 10, 2021. [Online]. Available: https://www.apple.com/

[67] "BIO-RAD." Accessed: Dec. 27, 2021. [Online]. Available: https://www.bio-rad.com/

[68] "Sino Biological." Accessed: Dec. 27, 2021. [Online]. Available: https://www.sinobiological.com/